

Imaging and Spectroscopy of Ultra Steep Spectrum Radio Sources ^{*}.

Carlos G. Bornancini^{1,2}, Carlos De Breuck³, Wim de Vries^{4,5}, Steve Croft^{4,6}, Wil van Breugel^{4,6}, Huub Röttgering⁷ and Dante Minniti⁸

¹ *Grupo de Investigaciones en Astronomía Teórica y Experimental, IATE, Observatorio Astronómico, Universidad Nacional de Córdoba, Laprida 854, X5000BGR, Córdoba, Argentina.*

² *Secretaría de Ciencia y Técnica de la Universidad Nacional de Córdoba.*

³ *European Southern Observatory, Karl Schwarzschild Straße 2, D-85748 Garching, Germany.*

⁴ *Institute of Geophysics and Planetary Physics, Lawrence Livermore National Laboratory L-413, 7000 East Avenue, Livermore, CA 94550, USA*

⁵ *University of California, Davis, 1 Shields Avenue, Davis, CA 95616, USA*

⁶ *University of California, Merced, P.O. Box 2039, Merced, CA 95344, USA*

⁷ *Leiden Observatory, PO Box 9513, 2300 RA, Leiden, The Netherlands*

⁸ *Pontificia Universidad Católica de Chile, Departamento de Astronomía y Astrofísica, Casilla 306, Santiago 22, Chile*

2 January 2018

ABSTRACT

We present a sample of 40 Ultra Steep Spectrum (USS, $\alpha \leq -1.3$, $S_\nu \propto \nu^\alpha$) radio sources selected from the Westerbork in the Southern Hemisphere (WISH) catalog. The USS sources have been imaged in K -band at the Cerro Tololo Inter-American Observatory (CTIO) and with the Very Large Telescope at Cerro Paranal. We also present VLT, Keck and William Herschel Telescope (WHT) optical spectroscopy of 14 targets selection from 4 different USS samples. For 12 sources, we have been able to determine the redshifts, including 4 new radio galaxies at $z > 3$. We find that most of our USS sources have predominantly small ($< 6''$) radio sizes and faint magnitudes ($K \gtrsim 18$). The mean K -band counterpart magnitude is $\overline{K} = 18.6$. The expected redshift distribution estimated using the Hubble $K-z$ diagram has a mean of $\overline{z}_{exp} \sim 2.13$, which is higher than the predicted redshift obtained for the SUMSS-NVSS sample and the expected redshift obtained in the 6C** survey. The compact USS sample analyzed here may contain a higher fraction of galaxies which are high redshift and/or are heavily obscured by dust. Using the 74, 352 and 1400 MHz flux densities of a sub-sample, we construct a radio colour-colour diagram. We find that all but one of our USS sources have a strong tendency to flatten below 352 MHz. We also find that the highest redshift source from this paper (at $z = 3.84$) does not show evidence for spectral flattening down to 151 MHz. This suggests that very low frequency selected USS samples will likely be more efficient to find high redshift galaxies.

Key words: surveys – radio continuum: general – radio continuum: galaxies – galaxies: high-redshift

1 INTRODUCTION

Distant powerful radio sources represent excellent targets to study evolutionary processes related to massive galaxies and their associated surrounding structures at high redshifts (e.g. De Breuck et al. 2002b; Miley et al. 2004; Overzier et al. 2006; Villar-Martín et al. 2003; Nesvadba et al. 2006). The most effective method for finding high-redshift radio galaxies is by selecting for Ultra Steep-Spectrum radio sources (USS, $\alpha \leq -1$, $S_\nu \propto \nu^\alpha$). A possible explanation of this empirical method is a K -

^{*} Based on observations obtained at Cerro Tololo Inter-American Observatory, a division of the National Optical Astronomy Observatories, which is operated by the Association of Universities for Research in Astronomy, Inc. under cooperative agreement with the National Science Foundation. Based on observations with the Very Large Telescope, obtained at the European Southern Observatory in Chile under Proposals 65.O-0125(A), 66.A.0006(B) and 69.A-0337(A).

correction induced by a curvature of the radio spectra. High redshift sources with concave radio spectra will have steeper spectral indices compared to those at low redshift (Krolik & Chen 1991; Carilli et al. 1999; Gopal-Krishna 1988). Comparing the extremely steep spectral index sources associated with galaxies residing closest to the cluster centres, Klamer et al. (2006) found an explanation that suggests that the steeper spectra can also be explained by pressure-confined radio lobes which have slow adiabatic expansion losses in high density environments. High-redshift radio galaxies are extremely luminous, and spatially extended, compared to normal galaxies at similar redshifts. The tight $K - z$ relation of radio galaxies in the Hubble K diagram suggest that these objects are amongst the most massive systems at each redshift (De Breuck et al. 2002b; Jarvis et al. 2001; Willott et al. 2003; Eales & Rawlings 1993; Lacy et al. 2000). Using the $K - z$ diagram and galaxy evolution models, Rocca-Volmerange et al. (2004) found that the typical hosts of radio galaxies correspond to the most massive elliptical galaxies with baryon masses $M \sim 10^{12} M_{\odot}$.

There is increasing new evidence that distant radio galaxies represent massive forming systems. Miley et al. (2006) found more than 10 individual clumpy features, possible satellite galaxies in the process of merging, in a region of 50×40 kpc around the radio galaxy MRC 1138–262 at $z = 2.2$. From a large VLT program, searching Ly α emitters around a sample of $2 < z < 5.2$ radio galaxies, Venemans et al. (2006) found that at least six of eight fields studied are overdense in Ly α emitters by a factor of 3–5 compared to the field. Some radio-galaxies, selected with the USS criterion, are surrounded by giant Ly α haloes. The size of these gas structures (100–200 kpc) are similar to the observed size of cD haloes in galaxies in nearby clusters (Reuland et al. 2003a; van Breugel et al. 2006). From a spatial cross-correlation analysis between USS at $0.5 < z < 1.5$ and surrounding $K < 20$ galaxies, Bornancini et al. (2006) found a comoving correlation length comparable to those obtained for clusters of galaxies with masses in the range $M \sim 10^{14} M_{\odot}$ in a cosmological N-body simulation. In this paper we present K -band observations, high-resolution radio maps and optical spectroscopy for a subsample of southern Ultra Steep Spectrum Radio Sources selected from the Westerbork in the Southern Hemisphere (WISH, De Breuck et al. (2002a)) 352 MHz catalog. We also present optical spectroscopy of sources selected from the De Breuck et al. (2000) and WISH USS samples, yielding 12 new redshifts, including four new radio galaxies at $z > 3$. These provide excellent targets for follow-up observations in this interesting redshift range.

The structure of this paper is organized as follows: Section 2 describes the sample analyzed. We describe the near-IR observations and data reductions in Section 3. Section 4 presents the near-IR identification and source extraction. We describe optical spectroscopy observations in Section 5 and discuss our results in Section 6. Finally, Section 7 presents the main conclusions.

In this work we assume a standard Λ CDM model Universe with cosmological parameters, $\Omega_M = 0.3$, $\Omega_{\Lambda} = 0.7$ and a Hubble constant of $H_0 = 100 \text{ Km s}^{-1} \text{ Mpc}^{-1}$.

2 SAMPLE DEFINITION

The USS sample was selected from the 352 MHz Westerbork In the Southern Hemisphere catalogue (De Breuck et al. 2002a). We used a selection criterion based on the radio properties of the sources, steep radio spectral index ($\alpha_{352}^{1400} < -1.3$) and small angular size ($< 30''$, as measured on the VLA maps). All of the first and most of the second priority targets have been observed. A detailed description of the radio observations and data reduction can be found in De Breuck et al. (2002a). Most of the targets selected for optical spectroscopy are selected from the USS samples of De Breuck et al. (2000).

3 OBSERVATIONS AND DATA REDUCTION

3.1 Radio Imaging

3.1.1 VLA

In order to obtain high resolution radio maps and accurate positions, we used the Very Large Array (VLA) of the National Radio Astronomy Observatory in the hybrid BnA-configuration at 1.4 GHz. The images were obtained on 1999 October 16 and 20 and consisted of L-band short subscans of 3 minutes each. We used the standard data reduction recipes in the Astronomical Image Processing Software (*AIPS*) package, including self-calibration for phase corrections.

3.2 K-band Imaging

3.2.1 CTIO

The USS fields were observed during two runs in 2000 March and 2001 January using the Ohio State InfraRed Imager/Spectrometer (OSIRIS) imager on the 4-meter V.M. Blanco telescope at the Cerro Tololo Inter-American Observatory (CTIO). OSIRIS is a 0.9–2.4 μm camera with a 1024×1024 HAWAII HgCdTe CCD array. We used a focal ratio of f/7 which resulted in a respective pixel size of $0''.161$. Individual frames were obtained as a co-addition of a number of single exposures with different integration times, in this way one effectively removes row/column related defects. For example, for sources with total exposures times of 1920s, we use 12 single exposures of 10s observed with a 16-point dithering pattern. This results in $16 \times 10 \times 12 = 1920\text{s} = 32$ minutes on source. We used similar procedure for the other images, doing small changes in the number of points of the dithering pattern and the exposure times for single observations. During the observations, tip-tilt mirror corrections were made. This resulted in typical FWHMs on the individual pointing frames ($12 \times 10\text{s}$ co-added) of $0''.5$ to $0''.7$. The mean was around $0''.6$ for the nights 2000 March 20 to 22, and around $0''.7$ on the 2001 January run.

A subsample of USS sources was observed in 1999 July with the Cerro Tololo IR imager (CIRIM) camera at the CTIO 4-meter V.M. Blanco telescope. The CCD detector is a 256×256 HgCdTe NICMOS 3 array with a pixel scale of $0''.414$ using a focal ratio of f/7.5. For these observations we obtained a mean FWHM of $1''.1$.

3.2.2 VLT

Seven sources undetected in the CTIO images were observed with the Infrared Spectrometer And Array Camera (ISAAC; Moorwood et al. 1998) on the Very Large Telescope (VLT) at Paranal, (Chile) between 2002 April and September. A K_s filter (2.0-2.3 μm) was used. The pixel scale was $0''.148$ per pixel. All the images were obtained under optimum seeing conditions with FWHM in the range $0''.7$ and $1''.0$, and a number of standard stars were observed during the same nights. In Table 1 we present the log of the near-IR observations, with the observation dates, telescope/instrument used and the total exposure times for all the USS sample.

3.2.3 Data Reduction

Data were reduced within IRAF¹, using the standard DIMSUM (Stanford et al. 1995) near-IR reduction package, including dark subtraction, flat fielding, sky-subtraction, bad pixel masking, bright object masking, registration and summing.

VLT images were reduced with ISAAC pipeline recipes 5.4.2² using the command line utility `EsoRex`, which includes standard routines, including dark correction, flat field calibration, bad pixel cleaning, image correlation and recombination.

3.2.4 Astrometry

The astrometric calibration of the images was performed using the WCStools package³ (Mink 2006), using the Two Micron All Sky Survey (2MASS) Catalogue of Point Sources a reference catalog (Cutri et al. 2003) and the USNO-A2.0 Catalogue (Monet et al. 1998) for fields with a few number of 2MASS sources. We estimate the uncertainty in the relative astrometry to be $\sim 0''.4$ - $0''.6$.

3.2.5 Photometry

The photometry for the CTIO observations was calibrated using 2MASS point sources detected in these fields. For VLT runs, magnitudes were calibrated using NICMOS near-infrared standards (Persson et al. 1998). All standard star magnitudes were obtained using SExtractor (Bertin & Arnouts 1996) with an aperture diameter of $6''$, which proved to be adequate by monitoring the growth curve of all the measured stars. For the observations made with OSIRIS and CIRIM at CTIO the K -band zero point was 22.64 ± 0.06 and 22.01 ± 0.02 (for 1 count/second, integrated over the source), respectively. For the ISAAC/VLT observations we derive the zero-point based on observations of the near-IR photometric standard star S301-D taken from the list of Persson et al. (1998). The zero-point obtained was 24.18 ± 0.01 . The zero-points do not include the airmass term, because the airmass dependence in K -band is small and we have observed all our objects with airmasses < 1.3 , with a mean of 1.06.

Because of the large uncertainties in the photometry, we did not correct the K -band magnitudes for Galactic extinction. We have used the NED Database⁴, which are based on the $E(B - V)$ values from the extinction maps of Schlegel et al. (1998). We found that most of the sources have values from 0.01 to 0.1, which are negligible compared to magnitude errors.

4 SOURCE DETECTION AND NEAR-IR IDENTIFICATION

We have identified the near-IR counterparts to the radio sources by overlaying the radio contour maps on to the K -band images using the *AIPS* task KNTR.

We measured the magnitudes of these identifications using SExtractor. The parameters were set such that, to be detected, an object must have a flux in excess of 1-1.5 times the local background noise level over at least N connected pixels, according to the seeing conditions and image qualities. In order to improve the detections of faint sources, we smoothed the K -band images using a circular Gaussian of FWHM=1-2 pixels. In some cases, we find that it is possible that the identification does not fall at the midpoint of the radio lobes, for radio sources with double or multiple components.

We measured magnitudes for all radio source identifications using SExtractor and circular apertures with diameters of $2''.0$, $4''.0$ and $8''.0$. We also obtained `MAG_BEST` magnitudes in order to facilitate comparison with the literature (Bornancini et al. 2004, 2006). This is usually equal to `MAG_AUTO`, but if the contribution of other source exceeds 10%, it is `MAG_ISOCOR`. The uncertainties quoted represent our best estimates, which includes the zero-point uncertainty (See Table 2).

Table 2 lists our USS sample, the columns are: IAU J2000 designation, spectral index obtained between 352 MHz and 1.4 GHz, largest angular size, as measured from radio maps taken with the VLA, aperture magnitudes in $2''.0$, $4''.0$ and $8''.0$, SExtractor `MAG_BEST` magnitudes, J2000 position coordinates of the radio source and the K -band identification counterpart, the half-light radius and `CLASS_STAR` values of the K -band identifications. SExtractor `CLASS_STAR` parameter provides an indication of the likelihood of an object being a galaxy or a star. In the ideal cases a galaxy has `CLASS_STAR`= 0.0 and a point source has `CLASS_STAR`= 1.0. We find that all the USS sample analyzed in this work are consistent with extended sources (galaxies) rather than point sources (stars or quasars).

We also considered studying the environments of these USS radio galaxy candidates. The environments of twenty USS sources observed with CTIO/OSIRIS were analyzed in Bornancini et al. (2004). In those images, only 7 radio galaxies were identified, finding a statistically significant signal of clustering. In Bornancini et al. (2006), a similar analysis was performed on a wider field and with deeper data, finding a stronger result. We therefore do not analyze the environments of the USS sources in the relatively shallow K -band images from this paper.

¹ Image Reduction and Analysis Facility (IRAF), a software system distributed by the National Optical Astronomy Observatories (NOAO)

² Available at <ftp://ftp.eso.org/pub/dfs/pipelines/isaac/>

³ Available at <ftp://cfa-ftp.harvard.edu/pub/gsc/WCSTools/>

⁴ <http://nedwww.ipac.caltech.edu/> - the NASA-IPAC Extragalactic Database

5 OPTICAL SPECTROSCOPY

During the past 6 years, we have obtained optical spectroscopy of 14 USS sources. The targets were mostly selected from 4 different USS samples: the 3 sub-samples of De Breuck et al. (2000) and the WISH–NVSS sample described in this paper. From these samples, we mostly selected the final targets based on the RA range when telescope time was available.

5.1 VLT

Optical spectroscopy of a subsample of USS sources were carried with FORS2 installed on the VLT Unit Telescope 4 Yepun between 2000 October and 2001 May. We used a similar data reduction strategy to De Breuck et al. (2006). We removed cosmic rays using the IRAF task `szap`, after bias and flatfield correction. We used the IRAF task `background` in order to remove sky variations and we extracted the spectra using a width appropriate to contain all flux in the extended emission lines. Finally we calibrated the one dimensional spectra in wavelength and flux. We used the procedures described in Röttgering et al. (1997) and in De Breuck et al. (2006) to determine the central wavelength, total line flux, deconvolved widths, and rest-frame equivalent widths (with their related errors) of all the emission and absorption lines detected in our spectra. For each object, we quote a single redshift, which is an average of all the lines, weighted by the uncertainties due to the line fitting and wavelength calibration. In Table 4 we show the measured parameters of the emission/absorption lines in the spectra.

5.2 Keck

Longslit observations were made on UT 2004 January 19–20, using the Low Resolution Imaging Spectrometer (LRIS; Oke et al. 1995) on Keck I, with a slit width of $1''.5$, under photometric conditions and $0''.8$ seeing. The spectroscopic setup is described in Table 3. Data reduction was performed in IRAF; data were bias-subtracted, response-corrected, cosmic-ray-zapped using Pieter van Dokkum’s LACosmic routine⁵, sky-subtracted, and spectra extracted in a $1''.5$ aperture. The resultant 1-D spectra were wavelength and flux calibrated using appropriate arcs and standard stars.

5.3 WHT

On UT 2006 December 14 and 15, we obtained 3 spectra using the ISIS double beam spectrograph (Carter et al. 1994) at the 4.2 m William Herschel telescope (WHT) at Observatorio Roque de los Muchachos on the Canary island of La Palma. Conditions were photometric with $0''.5$ and $1''.5$ seeing during the first and second night, respectively. We used a dichroic splitting the light at 5300 \AA and a $1''.5$ wide slit. The grisms used were the R300B in the blue arm and the R316R in the red arm. None of the 3 objects were detected in the blue arm. In the red arm, only

WN J0912–1655 was clearly detected in 5400 s of observing time. WN J0604–2015 and WN J0610+6611 were not detected in 5400 s and 7200 s, respectively. We extracted the red spectrum of WN J0912–1655 with an aperture width of $2''.4$.

5.4 Results

We have determined redshifts of 12 out of 14 targets observed. The two targets without redshifts were undetected in 1.5 to 2 hours on a 4 m telescope, and need long integration on 8–10 m class telescopes. Apart from TN J2009–3040, which is a $z=3.158$ quasar, all 11 targets are radio galaxies with redshifts from $z=0.550$ to $z=3.837$. Five of the radio galaxies are at $z>2$, including three at $z>3$. Table 4 lists the emission line parameters of all targets. The 10 new redshifts from the De Breuck et al. (2000) USS sample raises the number of spectroscopic observations from that sample from 46 to 56, and the number of known redshifts from 34 to 44.

6 DISCUSSION

6.1 Correlations

In this work we have excluded large radio sources because those are most likely foreground objects and not at high redshift. In Figure 1 we present the correlation between largest angular size (LAS) and the K –magnitudes obtained within an aperture of $4''$. As can be seen most of the sources have small radio sizes with $LAS < 8''$. The vertical dashed line represent the expected K –band magnitude of a $z \sim 3$ source, indicating that high redshift sources have compact radio morphologies. Several authors have applied the small angular-size criterion in order to find high redshift radio galaxies (Blundell et al. 1998; Jarvis et al. 2004; Cruz et al. 2006). There are a few cases of radio galaxies at high redshifts with large angular sizes (4C 23.56 at $z=2.483$ has $LAS=53''$). However, Pedani (2003) found that the introduction of a strong angular size bias such as $LAS < 15''$, increases the efficiency in selecting high redshift radio galaxies by a factor of two.

Some radio galaxies have very faint or no K –band counterpart presenting large deviation in the Hubble $K - z$ diagram (De Breuck et al. 2006), and 20% of high-redshift radio galaxies fail to show optical emission lines in spectroscopy observations using the Keck Telescope (De Breuck et al. 2001; Reuland et al. 2003b). This could be an indication that some high redshift radio galaxies contain great amounts of dust. Willott et al. (2002) found an anti-correlation between dust emission (measured from $850 \mu\text{m}$ flux) and the projected linear size, though Reuland et al. (2004) did not confirm this using a larger sample of radio galaxies. It is likely that the compact USS sample analyzed here may also contain a mix of galaxies either at very high redshift, or heavily obscured by dust.

6.2 Expected redshift distribution

We have estimated the redshift of the USS sample using linear regression and the Hubble $K - z$ diagram of

⁵ <http://www.astro.yale.edu/dokkum/lacosmic/>

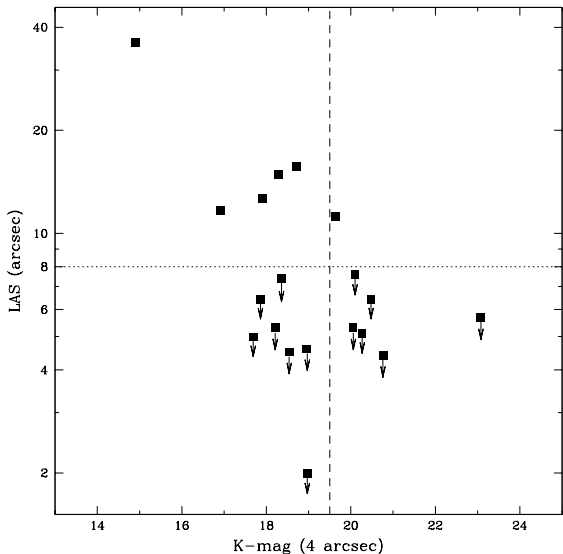


Figure 1. Radio largest angular size vs K -magnitudes ($4''$ aperture). Dashed line represent the expected K -band magnitude of a $z \sim 3$ source. Most of the sources have small radio sizes as indicated by the horizontal dotted line.

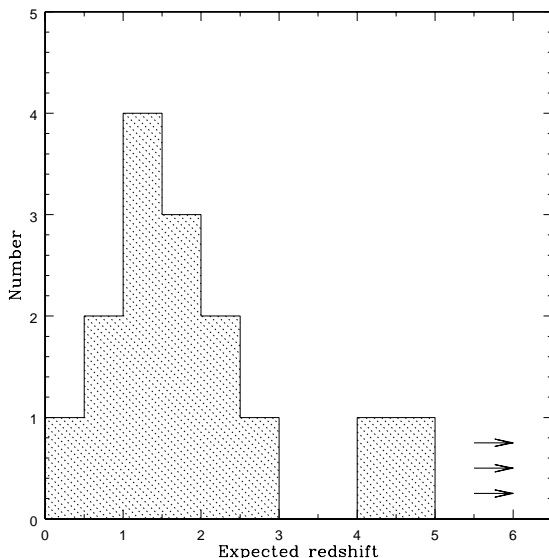


Figure 2. Distribution of expected redshift of USS sources, estimated from the Hubble $K-z$ diagram using 64 kpc metric apertures.

De Breuck et al. (2002b). Using aperture photometry in a 64 kpc metric aperture, De Breuck et al. (2002a) found $K = 4.633 \times \log_{10}(z) - 17.266$. As we expect most radio galaxies to have $1 < z < 4$, we have assumed $K_{64kpc} = K(8'')$, as $8''$ corresponds to ~ 64 kpc at $z=1$, which only a small dependence on redshift $z > 1$ in our adopted Cosmology. Figure 2 shows the expected redshift distribution for our USS sample. The median predicted redshift is $\bar{z}_{exp}=2.13$, which is higher than the predicted redshift obtained by De Breuck et al.

(2004) for the SUMSS–NVSS sample ($\bar{z}_{sumss} = 1.75$) and the expected redshift obtained in the 6C* ($z \sim 1.9$; Jarvis et al. 2001) and 6C** surveys ($z \sim 1.7$; Cruz et al. 2007).

In Figure 4 we show the K -band magnitude distribution of USS sources, measured in a $8''$ diameter aperture. We compare our results with those obtained in the SUMSS–NVSS (De Breuck et al. 2004), 6C** (Cruz et al. 2007) catalogues and data selected at 74 MHz taken from Jarvis et al. (2004). The mean K -band magnitudes in an $8''$ diameter aperture of the USS is $\bar{K}=18.58$, which is one magnitude fainter than those obtained by De Breuck et al. (2004) in the SUMSS–NVSS survey ($\bar{K}=17.57$) and by Cruz et al. (2006) in the the 6C** survey ($\bar{K}=17.59$). We find a similar result using BEST magnitudes. Our USS sample has $\bar{K}_{BEST}=18.74$, and from a similar study Bornancini et al. (2006) found $\bar{K}_{BEST}=17.97$. The fainter K -band counterparts of the WISH–NVSS USS sources could be an indication that the host galaxies are located either at higher redshifts (i.e. a more efficient selection), or in a very dense, dusty medium.

Alternatively, the WISH–NVSS USS radio galaxies are intrinsically less massive and hence less luminous than the ones in previous samples. This could be due to the fainter flux limits probed in this sample. However, using *Spitzer* rest-frame near-IR photometry, Seymour et al. 2007 do not find a strong dependence of host galaxy mass on 3 GHz radio luminosity, so we regard this explanation as unlikely given the small difference in radio luminosity between the USS samples.

Alternatively, the WISH–NVSS USS sources may be less massive and hence fainter in the observed K -band. This may be because WISH–NVSS sources have fainter radio fluxes than most previous USS samples. Such a radio power dependence in the $K-z$ diagram has been suggested by various authors (Eales et al. 1997; Best et al. 1998; Jarvis et al. 2001; De Breuck et al. 2002b; Willott et al. 2002). However, using *rest-frame* near-IR imaging of a sample of 69 radio galaxies at $z > 1$ observed with *Spitzer*, Seymour et al. (2007) do not find a strong dependence of host galaxy mass on 3 GHz radio luminosity, so we regard this explanation as unlikely given the small difference in radio luminosity between the USS samples.

6.3 Radio two-colour diagram and spectral curvature

We use the CATS database of the Special Astronomy Observatory (Verkhodanov et al. 1997) to search for radio measurements in order to study the radio spectral energy distribution at low frequencies. Figure 3 shows the radio two-colour diagram, which compares the spectral indices at 74–352 MHz and 352–1400 MHz for 12 USS sources of the total sample (Filled circles). Fluxes at 74 MHz were obtained from the VLA Low-frequency Sky Survey (Cohen et al. 2006). The line indicates the relation for USS sources whose spectra follow a single power law from 74 to 1400 MHz. Open circles represent measurements obtained using the WENSS–NVSS sample at 325 MHz and 1.4 GHz taken from De Breuck et al. (2000). We find a general agreement with those values. Only a single source in our sample is consistent with a straight spectrum, and it is clear that most of the USS sources have substantially flatter spectral indices between 74 and 352

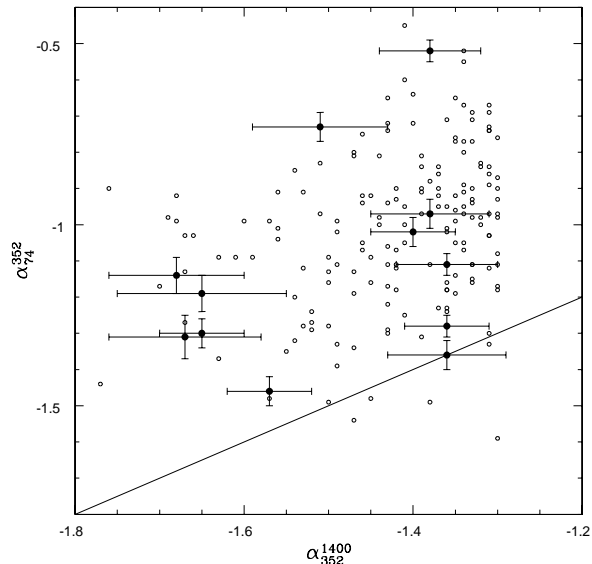


Figure 3. Radio two-colour diagram for USS sources in our sample (filled circles). Open circles represent measurements obtained using the WENSS–NVSS sample at 325 MHz and 1.4 GHz taken from De Breuck et al. (2000). The line indicates the relation for USS sources whose spectra follow a single power law from 74 to 1400 MHz.

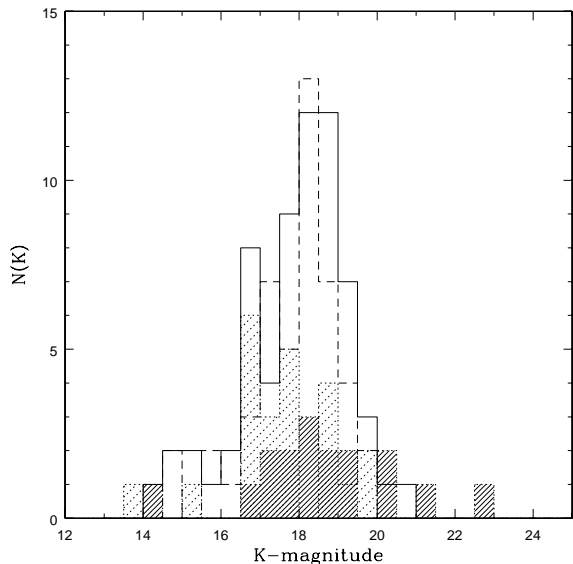


Figure 4. K -band magnitude distribution of USS sources, measured in a $8''$ diameter aperture (shaded histogram). Solid and dashed lines represent the distribution of K -band magnitude, measured in a $8''$ diameter aperture for sources detected in the SUMSS–NVSS (De Breuck et al. 2004) and 6C** (Cruz et al. 2007) catalogues. Dotted histogram represent USS sources selected at 74 MHz taken from Jarvis et al. (2004).

MHz than between 352 and 1400 MHz. The median spectral index obtained at 74–352 MHz is $\bar{\alpha}_{74}^{352} = -1.1$, while the median at high frequencies is $\bar{\alpha}_{352}^{1400} = -1.5$. The spectral flattening is in the range $0 < \Delta(\alpha) < 0.8$. Unfortunately, we do not have redshifts for any of the 12 sources with 74 MHz data. However, WN J2007-1316 at $z=3.837$ is detected in the Mauritius Southern Sky Survey (Pandey 2006) with $S_{151\text{MHz}}=3.58\pm 0.57$ Jy. This implies $\alpha_{151}^{352}=-1.60\pm 0.19$, compared to $\alpha_{352}^{1400}=-1.52\pm 0.04$. Although the uncertainty in the spectral index is larger than for the 74–352 MHz data, this result suggests that the highest redshift radio galaxy confirmed in our sample does retain a straight radio spectrum through the lowest frequencies observed. As noted by Klammer et al. (2006) $\sim 90\%$ of USS sources selected from the SUMSS and NVSS catalogues show a straight radio spectra characterised by a single power law beyond ~ 1 GHz. At frequencies below 100 MHz spectral curvature is much more common than at higher frequencies due principally to synchrotron self-absorption. This suggests that very low frequency selected USS samples will be likely to be more efficient to find high redshift galaxies.

7 CONCLUSIONS

We present K -band observations obtained with CTIO at Cerro Tololo and with VLT at Cerro Paranal, high-resolution VLA radio maps for a sample of 28 Ultra Steep Spectrum Radio Sources selected from the WISH catalog. We also present optical spectroscopy from VLT/FORS2, Keck/LRIS and WHT/ISIS for 12 USS sources, mainly from the De Breuck et al. (2000) samples.

We find that most of our USS sources have small radio sizes and fainter magnitudes. The mean K -band counterpart magnitude measured in $8''$ diameter aperture is $\bar{K}=18.58$, which is one magnitude fainter than those obtained on the literature. The expected redshift distribution estimated using the Hubble $K-z$ diagram has a mean of $\bar{z}_{exp}=2.13$, which is higher than the predicted redshift obtained for the SUMSS–NVSS sample and the expected redshift obtained in the 6C* and 6C** surveys.

From our spectroscopy, we identify one $z=3.158$ quasar, and 11 new radio galaxies, 3 of which are at $z>3$.

From a radio colour-colour diagram of a subsample of 12 sources, we find that all but one radio spectra flatten significantly below 352 MHz. We also find that the highest redshift source from this paper (at $z=3.84$) does not show evidence for spectral flattening down to 151 MHz. Because most low redshift radio galaxies have a flatter spectra below 352 MHz, selecting USS sources at low frequencies is likely to be more efficient selection technique to find high redshift galaxies. The forthcoming low frequency observatories such as LOFAR, LWA or SKA will be enable to find large samples of low-frequency selected USS sources (e.g. Rottgering et al. 2006) and will therefore open new perspectives on the nature and evolution of high redshift radio galaxies.

8 ACKNOWLEDGMENTS

We are grateful to the anonymous referee for his/her careful reading of the manuscript and a number of comments,

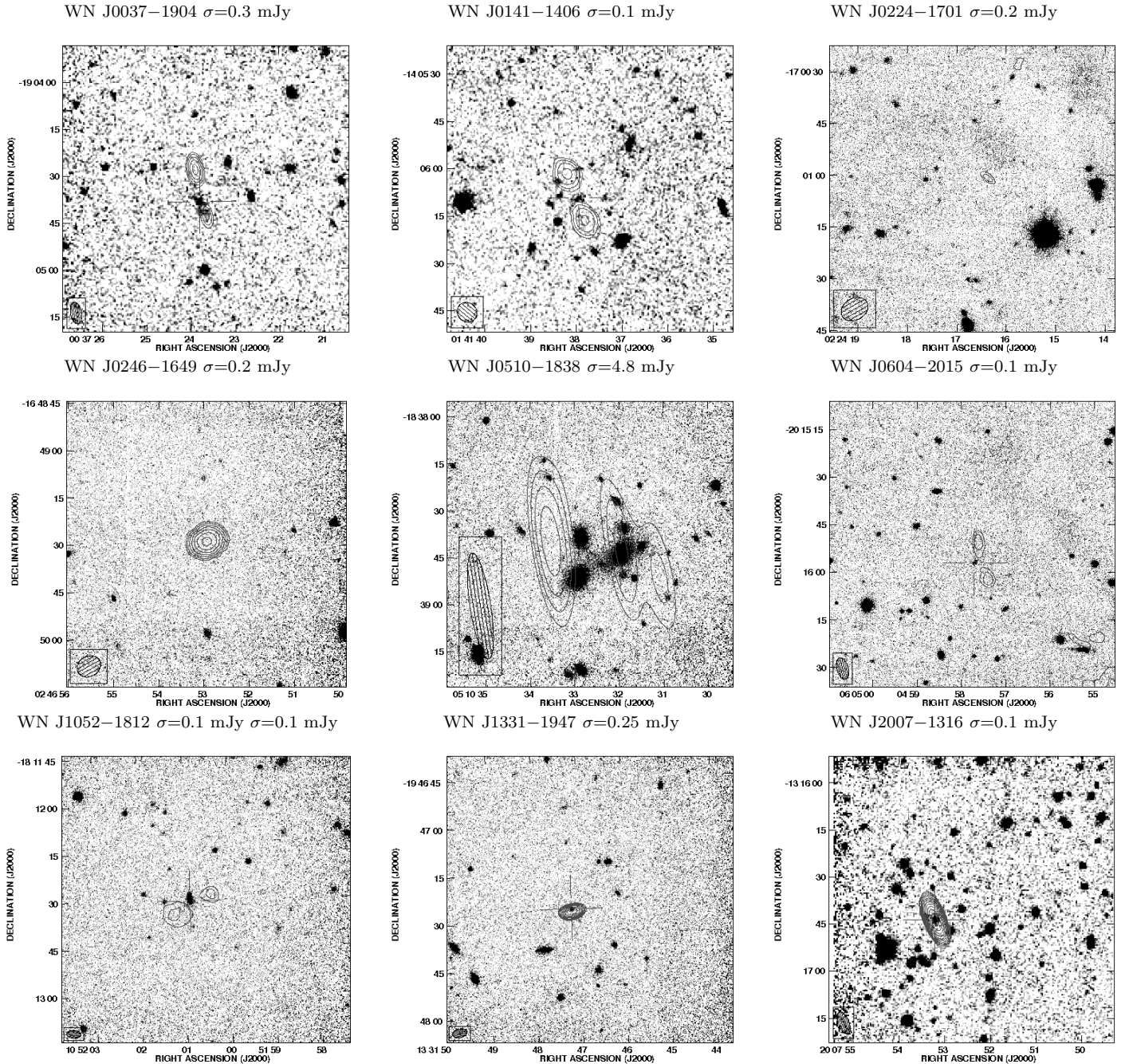


Figure 5. Part of the K -band images of the WISH sample from observation of CTIO/OSIRIS, CTIO/CIRIM or VLT/ISAAC, with radio contours overlaid. The contours represent the VLA radio emission at 1.4 GHz. The contour scheme is a geometric progression in $\sqrt{2}$, which implies a factor two change in surface brightness every 2 contours. The first contour level is at $3\sigma_{\text{rms}}$, where σ_{rms} is the rms noise measured around the sources, which is indicated above each plot. The half-power beamwidth is indicated in the lower left corner of the plots. The open cross indicates the K -band identification, as listed in Table 2. See <http://www.eso.org/~cbreuck/papers.html> for a version with all 28 overlays

which improved the paper. We thank Adam Stanford and Cyril Tasse for their help in taking the Keck and WHT spectra, respectively. This work was partially supported by the Consejo Nacional de Investigaciones Científicas y Técnicas (CONICET), the Secretaría de Ciencia y Técnica de la Universidad Nacional de Córdoba and the European Union Alfa II Programme, through LENAC, the Latin American-European Network for Astrophysics and Cosmology. The

work of WdV, WvB and SDC was performed under the auspices of the U.S. Department of Energy, National Nuclear Security Administration by the University of California, Lawrence Livermore National Laboratory under contract No. W-7405-Eng-48. Based on observations made with the European Southern Observatory telescopes obtained from the ESO/ST-ECF Science Archive Facility. The authors made use of the database CATS (Verkhodanov et

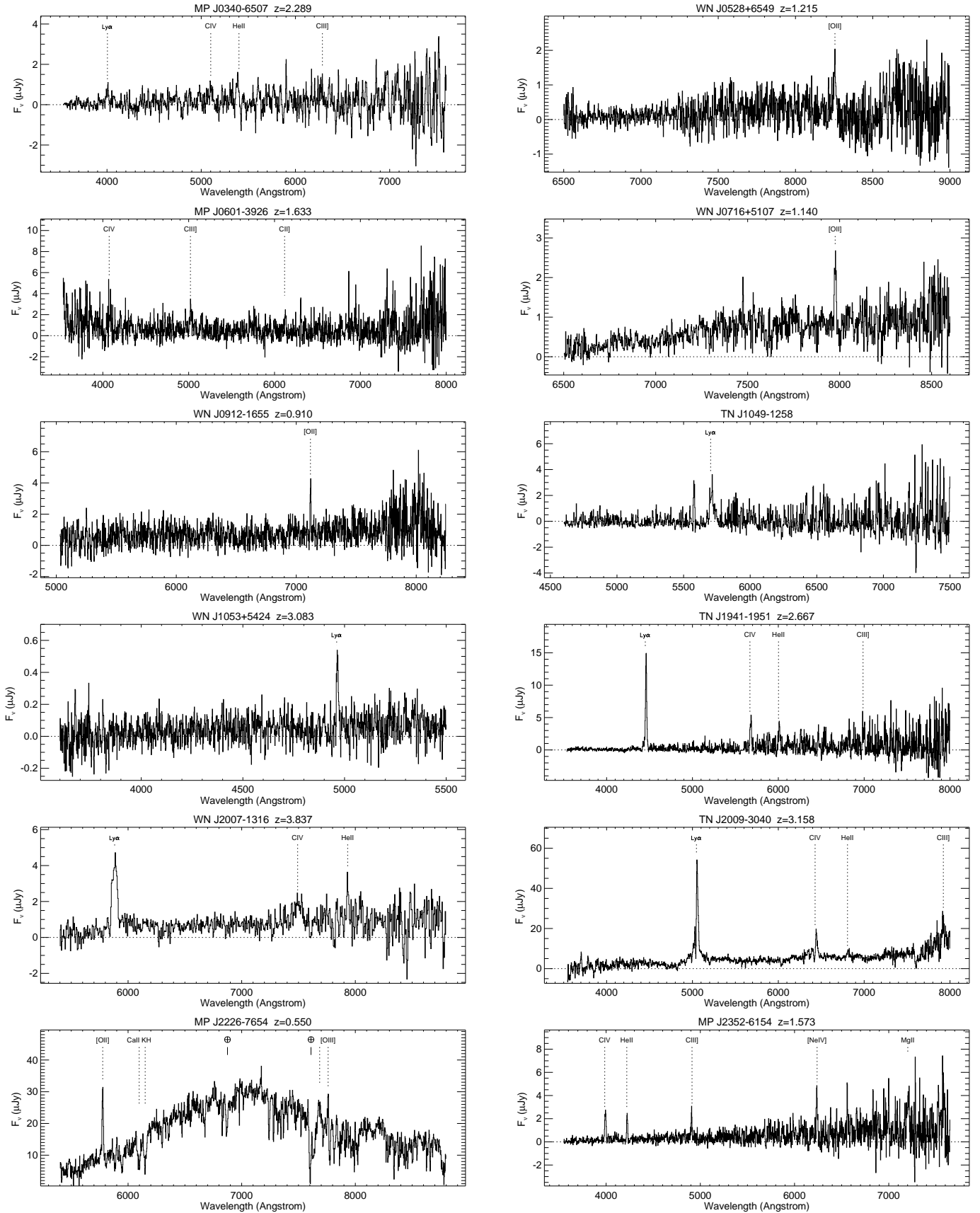


Figure 6. Optical spectroscopy of USS sources. Prominent features are indicated with vertical dotted lines showing the predicted observed wavelength of the lines at the redshift the source. Atmospheric absorption features are indicated with \oplus .

al. 1997) of the Special Astrophysical Observatory and the NASA/IPAC extragalactic database (NED) which is operated by the Jet Propulsion Laboratory, Caltech, under contract with the National Aeronautics and Space Administration. This publication makes use of data products from the Two Micron All Sky Survey, which is a joint project of the University of Massachusetts and the Infrared Processing and Analysis Center/California Institute of Technology, funded by the National Aeronautics and Space Administration and the National Science Foundation.

REFERENCES

- Bertin E., Arnouts S., 1996, *A & A Supp.* 117, 393.
- Best, P. N., Longair, M. S., & Roettgering, H. J. A. 1998, *MNRAS*, 295, 549
- Bornancini, C. G., Martínez, H. J., Lambas, D. G., de Vries, W., van Breugel, W., De Breuck, C., & Minniti, D. 2004, *AJ*, 127, 679
- Bornancini, C. G., Lambas, D. G., & De Breuck, C. 2006, *MNRAS*, 366, 1067
- Bornancini, C. G., Padilla, N. D., Lambas, D. G., & De Breuck, C. 2006, *MNRAS*, 368, 619
- Blundell, K. M., Rawlings, S., Eales, S. A., Taylor, G. B., & Bradley, A. D. 1998, *MNRAS*, 295, 265
- Carilli, C. L., Röttgering, H. J. A., Miley, G. K., Pentericci, L. H., & Harris, D. E. 1999, *The Most Distant Radio Galaxies*, 123
- Carter, D. et al. 1994, *ISIS Users' Manual*
- Cohen, A. S., Lane, W. M., Kassim, N. E., Lazio, T. J. W., Cotton, W. D., Perley, R. A., Condon, J. J., & Erickson, W. C. 2006, *Astronomische Nachrichten*, 327, 262
- Cruz, M. J., et al. 2006, *MNRAS*, 373, 1531
- Cruz, M. J., et al. 2007, *MNRAS*, in press, astro-ph/0612268
- De Breuck, C., van Breugel, W., Röttgering, H. J. A., & Miley, G. 2000, *A&AS*, 143, 303
- De Breuck, C., et al. 2001, *AJ*, 121, 1241
- De Breuck, C., Tang, Y., de Bruyn, A. G., Röttgering, H., & van Breugel, W. 2002b, *A&A*, 394, 59
- De Breuck, C., van Breugel, W., Stanford, S. A., Röttgering, H., Miley, G., & Stern, D. 2002a, *AJ*, 123, 637
- De Breuck, C., Hunstead, R. W., Sadler, E. M., Rocca-Volmerange, B., & Klamer, I. 2004, *MNRAS*, 347, 837
- De Breuck, C., Klamer, I., Johnston, H., Hunstead, R. W., Bryant, J., Rocca-Volmerange, B., & Sadler, E. M. 2006, *MNRAS*, 366, 58
- Cutri, R. M., Skrutskie, M. F., van Dyk, S., et al. 2003, *The 2MASS All-Sky Catalogue of Point Sources*
- Eales, S. A., & Rawlings, S. 1993, *ApJ*, 411, 67
- Eales, S., Rawlings, S., Law-Green, D., Cotter, G., & Lacy, M. 1997, *MNRAS*, 291, 593
- Gopal-Krishna 1988, *A&A*, 192, 37
- Jarvis, M. J., Rawlings, S., Eales, S., Blundell, K. M., Bunker, A. J., Croft, S., McLure, R. J., & Willott, C. J. 2001, *MNRAS*, 326, 1585
- Jarvis, M. J., Cruz, M. J., Cohen, A. S., Röttgering, H. J. A., & Kassim, N. E. 2004, *MNRAS*, 355, 20
- Klamer, I. J., Ekers, R. D., Bryant, J. J., Hunstead, R. W., Sadler, E. M., & de Breuck, C. 2006, *MNRAS*, 371, 852
- Krolik, J. H., & Chen, W. 1991, *AJ*, 102, 1659
- Lacy, M., Bunker, A. J., & Ridgway, S. E. 2000, *AJ*, 120, 68
- Miley, G. K., et al. 2004, *Nature*, 427, 47
- Miley, G. K., et al. 2006, *ApJ*, 650, L29
- Mink, D. 2006, *ASP Conf. Ser.* 351: *Astronomical Data Analysis Software and Systems XV*, 351, 204
- Moorwood, A., et al. 1998, *The Messenger*, 94, 7
- Monet, D. B. A., et al. 1998, *VizieR Online Data Catalog*, 1252, 0
- Nesvadba, N., Lehnert, M., Eisenhauer, F., Gilbert, A., Tecza, M., & Abuter, R. 2006, *ApJ*, 650, 693
- Oke, J. B., et al. 1995, *PASP*, 107, 375
- Overzier, R. A., et al. 2006, *ApJ*, submitted
- Pandey, V. 2006, *PhD thesis*, Raman Research Institute, Bangalore, India
- Pedani, M. 2003, *New Astronomy*, 8, 805
- Persson, S. E., Murphy, D. C., Krzemiński, W., Roth, M., & Rieke, M. J. 1998, *AJ*, 116, 2475
- Reuland, M., et al. 2003, *ApJ*, 592, 755
- Reuland, M., van Breugel, W., Röttgering, H., de Vries, W., De Breuck, C., & Stern, D. 2003, *ApJ*, 582, L71
- Reuland, M., Röttgering, H., van Breugel, W., & De Breuck, C. 2004, *MNRAS*, 353, 377
- Rocca-Volmerange, B., Le Borgne, D., De Breuck, C., Fioc, M., & Moy, E. 2004, *A&A*, 415, 931
- Röttgering, H. J. A., van Ojik, R., Miley, G. K., Chambers, K. C., van Breugel, W. J. M., & de Koff, S. 1997, *A&A*, 326, 505
- Röttgering, H., et al. 2006, in proceedings "Cosmology, galaxy formation and astroparticle physics on the pathway to the SKA", Oxford, astro-ph/0610596
- Schlegel, D. J., Finkbeiner, D. P., & Davis, M. 1998, *ApJ*, 500, 525
- Seymour et al. 2007 *ApJS*, in press, astro-ph/0703324
- Stanford, S. A., Eisenhardt, P. R. M., & Dickinson, M. 1995, *ApJ*, 450, 512
- van Breugel, W., de Vries, W., Croft, S., De Breuck, C., Dopita, M., Miley, G., Reuland, M., Röttgering, H. 2006, *Astronomische Nachrichten*, 327, 175
- Venemans, B. P. et al. 2006, *A&A* accepted
- Verkhodanov, O. V., Trushkin, S. A., & Chernenkov, V. N. 1997, *Baltic Astronomy*, 6, 275
- Villar-Martín M., Vernet J., di Serego Alighieri S., Fosbury R., Humphrey A., Pentericci L., 2003, *MNRAS*, 346, 273
- Willott, C. J., Rawlings, S., Archibald, E. N., & Dunlop, J. S. 2002, *MNRAS*, 331, 435
- Willott, C. J., Rawlings, S., Jarvis, M. J., & Blundell, K. M. 2003, *MNRAS*, 339, 173

Table 1. Log of the *K*-band observations of the USS WISH sample.

Name	Dates observed	Telescope/Instr.	Total exposure times (s)
WN J0037–1904	2001-01-09	CTIO/CIRIM	1920
WN J0141–1406	1999-07-20	CTIO/CIRIM	1500
WN J0224–1701	2002-07-07	VLT/ISAAC	2340
WN J0246–1649	2001-01-09	CTIO/OSIRIS	1920
WN J0510–1838	2001-01-09	CTIO/OSIRIS	960
WN J0604–2015	2002-09-02	VLT/ISAAC	2340
WN J0910–2228	2000-03-22	CTIO/OSIRIS	3840
WN J0912–1655	2000-03-21	CTIO/OSIRIS	1920
WN J1047–1836	2000-03-22	CTIO/OSIRIS	3840
WN J1052–1812	2000-03-23	CTIO/OSIRIS	1920
WN J1101–2134	2002-04-23	VLT/ISAAC	1440
WN J1109–1917	2000-03-23	CTIO/OSIRIS	1920
WN J1132–2102	2001-01-09	CTIO/OSIRIS	3720
WN J1138–1324	2002-04-23	VLT/ISAAC	2340
WN J1150–1317	2000-03-22	CTIO/OSIRIS	3840
WN J1222–2129	2000-03-21	CTIO/OSIRIS	3360
WN J1255–1913	2000-03-23	CTIO/OSIRIS	1920
WN J1331–1947	2000-03-23	CTIO/OSIRIS	1920
WN J1450–1525	2000-03-21	CTIO/OSIRIS	2160
WN J1516–2110	2002-04-23	VLT/ISAAC	2340
WN J1518–1225	2000-03-23	CTIO/OSIRIS	3840
WN J1557–1349	2000-03-22	CTIO/OSIRIS	1920
WN J1603–1500	2002-04-23	VLT/ISAAC	2340
WN J1637–1931	2000-03-21	CTIO/OSIRIS	1280
WN J2002–1842	2002-04-23	VLT/ISAAC	2340
WN J2007–1316	1999-07-20	CTIO/CIRIM	3840
WN J2214–2353	1999-07-20	CTIO/CIRIM	2880
WN J2343–1947	1999-07-20	CTIO/CIRIM	1920

Table 2. Results of the K -band and radio observations of the WISH–NVSS USS sample

Name	α_{352}^{1400}	LAS ($''$)	K(2 $''$) (mag)	K(4 $''$) (mag)	K(8 $''$) (mag)	K_{BEST} (mag)	$RA_{J2000}^{\text{radio}}$ h m s	$DEC_{J2000}^{\text{radio}}$ ° ' $''$	$RA_{J2000}^{K\text{-band}}$ h m s	$DEC_{J2000}^{K\text{-band}}$ ° ' $''$	$r_{1/2}$ ($''$)	S/G
WN J0037–1904	−1.36±0.04	14.9	19.05±0.09	18.30±0.09	17.56±0.09	17.38±0.09	00 37 23.8	−19 04 35.6	00 37 23.79	−19 04 38.37	0.36	0.02
WN J0141–1406	−1.68±0.05	15.7	19.54±0.19	18.71±0.18	18.80±0.33	18.50±0.22	01 41 38.0	−14 06 09.7	01 41 37.94	−14 06 09.17	0.25	0.11
WN J0224–1701	−1.36±0.08	8.2	...	>22.0	02 24 15.7	−17 01 10.3
WN J0246–1649	−1.38±0.04	<4.4	...	>23.0	02 46 52.9	−16 49 28.7
WN J0510–1838*	−1.65±0.04	36.1	15.63±0.01	14.90±0.01	14.35±0.01	14.05±0.10	05 10 32.2	−18 38 41.4	05 10 31.96	−18 38 44.00	2.62	0.03
WN J0604–2015	−1.51±0.04	11.2	20.23±0.06	19.63±0.06	19.14±0.08	19.54±0.08	06 04 57.4	−20 15 56.5	06 04 57.71	−20 15 57.01	0.95	0.00
WN J0910–2228*	−1.57±0.04	<2.0	19.35±0.16	18.97±0.21	19.04±0.37	18.93±0.17	09 10 34.1	−22 28 47.4	09 10 34.15	−22 28 47.13	0.72	0.00
WN J0912–1655	−1.58±0.06	<5.0	18.18±0.11	17.69±0.12	17.23±0.14	17.51±0.13	09 12 57.1	−16 55 55.5	09 12 57.17	−16 55 55.58	0.81	0.08
WN J1047–1836	−1.46±0.05	<4.5	18.94±0.13	18.54±0.15	18.28±0.21	18.58±0.15	10 47 15.5	−18 36 30.6	10 47 15.39	−18 36 30.32	0.64	0.02
WN J1052–1812	−1.52±0.05	11.7	17.45±0.08	16.91±0.09	16.65±0.10	16.98±0.08	10 52 00.8	−18 12 31.4	10 52 00.88	−18 12 30.08	0.98	0.01
WN J1101–2134	−1.67±0.07	<4.4	...	>21.0	11 01 54.2	−21 34 28.4
WN J1109–1917	−1.38±0.04	<4.4	20.27±0.41	20.76±1.17	...	20.26±0.37	11 09 49.9	−19 17 54.0	11 09 49.89	−19 17 53.66	0.34	0.39
WN J1132–2102	−1.42±0.04	<4.4	...	>23.0	11 32 52.7	−21 02 44.7
WN J1138–1324	−1.53±0.08	<4.6	...	>22.0	11 38 05.0	−13 24 22.7
WN J1150–1317	−1.37±0.04	<4.6	19.32±0.15	18.94±0.19	18.37±0.22	18.93±0.19	11 50 09.6	−13 17 54.1	11 50 09.52	−13 17 52.82	0.68	0.00
WN J1222–2129	−1.42±0.06	<4.5	...	>23.0	12 22 48.2	−21 29 11.1
WN J1255–1913	−1.67±0.06	<4.5	...	>23.0	12 55 52.4	−19 13 01.5
WN J1331–1947	−1.40±0.04	<6.4	18.15±0.11	17.86±0.13	17.86±0.21	17.88±0.13	13 31 47.2	−19 47 26.7	13 31 47.18	−19 47 25.87	0.57	0.52
WN J1450–1525	−1.42±0.11	<5.2	23.71±0.10	23.08±0.10	22.85±0.13	22.77±0.11	14 50 42.7	−15 25 39.2	14 50 42.58	−15 25 40.51	1.14	0.04
WN J1516–2110	−1.38±0.04	<5.4	...	>22.0	15 16 42.4	−21 10 27.7
WN J1518–1225	−1.67±0.06	<5.1	20.25±0.20	22.08±0.41	...	20.21±0.34	15 18 43.8	−12 25 30.6	15 18 43.48	−12 25 34.36	0.44	0.67
WN J1557–1349	−1.39±0.06	<5.3	18.64±0.13	18.21±0.16	18.59±0.35	18.32±0.17	15 57 41.5	−13 49 59.1	15 57 41.61	−13 49 57.63	0.70	0.03
WN J1603–1500	−1.44±0.05	<5.3	20.08±0.07	20.05±0.14	20.11±0.31	19.99±0.10	16 03 04.6	−15 00 53.0	16 03 04.65	−15 00 53.68	0.52	0.69
WN J1637–1931	−1.60±0.04	<5.5	...	>22.0	16 37 44.8	−19 31 24.2
WN J2002–1842	−1.42±0.06	<7.6	20.42±0.10	20.10±0.16	21.07±0.77	20.21±0.13	20 02 56.0	−18 42 46.3	20 02 55.99	−18 42 46.25	0.58	0.22
WN J2007–1316	−1.52±0.04	<7.4	18.75±0.05	18.36±0.07	18.08±0.09	18.25±0.07	20 07 53.2	−13 16 43.7	20 07 53.22	−13 16 43.70	0.77	0.57
WN J2214–2353	−1.34±0.05	12.7	18.62±0.05	17.90±0.05	17.37±0.06	17.64±0.05	22 14 14.0	−23 53 24.8	22 14 14.17	−23 53 27.46	1.63	0.03
WN J2343–1947	−1.80±0.04	<6.4	21.07±0.19	20.48±0.22	20.42±0.39	20.09±0.22	23 43 16.3	−19 47 15.4	23 43 16.23	−19 47 15.83	1.13	0.00

* ATCA image (De Breuck et al. 2000)

Table 3. Log of the Keck I optical spectroscopy.

Target	Dichroic	Blue grism	Blue pix. scale	Resolution	Red grating	Red pix. scale	Resolution	Exp. time	PA
WN J0528+6549	D680	400/3400	1.04 Å / pix	9.5Å	400/8500	1.86Å / pix	8.1Å	1 × 1800 s	177.00
WN J0716+5107	D680	400/3400	1.04 Å / pix	9.5Å	400/8500	1.86Å / pix	8.1Å	2 × 1800 s	201.00
WN J1053+5424	D560	300/5000	1.43 Å / pix	12Å	400/8500	1.86Å / pix	8.1Å	4 × 1800 s	254.06

Table 4. Emission line measurements

Source	z	Line	λ_{obs} Å	Flux 10^{-16} erg s $^{-1}$ cm $^{-2}$	Δv_{FWHM} km s $^{-1}$	$W_{\lambda}^{\text{rest}}$ Å
MP J0340–6507	2.289±0.005	Ly α	4000±4	0.40±0.05	1860±640	>65
		C IV λ 1549	5100±27	0.15±0.05	2300±1800	20±10
		He II λ 1640	6275±10	0.26±0.05	1400±500	>40
		C III] λ 1909	6270±10	0.25±0.05	1600±1100	>130
WN J0528+6549	1.217±0.005	[O II] λ 3727	8263±17	0.09±0.02	1400±900	>31
MP J0601–3926	1.633±0.001	C IV λ 1549	4083±27	0.30±0.15	2300±1600	>4
		C III] λ 1909	5020±4	0.6±0.1	1200±500	28±6
		C II] λ 2326	6130±4	0.20±0.04	550±360	20±7
WN J0716+5107	1.1401±0.0002	[O II] λ 3727	7976±1	0.06±0.01	<500	8±1
WN J0912–1655	0.9102±0.0002	[O II] λ 3727	7119±1	0.10±0.02	<100	11±2
TN J1049–1258	3.697±0.004	Ly α	5712±5	0.6±0.1	1600±500	>63
WN J1053+5424	3.083±0.001	Ly α	4965±1	0.06±0.01	<500	25±6
TN J1941–1951	2.667±0.001	Ly α	4460±1	3.7±0.4	800±200	330±70
		C IV λ 1549	5680±2	0.9±0.1	850±200	64±20
		He II λ 1640	6010±3	0.4±0.1	850±300	23±6
		C III] λ 1909	7000±16	0.2±0.1	1000±700	10±4
WN J2007–1316	3.837±0.001	Ly α	5883±3	1.8±0.2	2400±300	77±13
		C IV λ 1549	7500±20	0.5±0.1	3100±1700	26±5
		He II λ 1640	7933±2	0.2±0.1	450±200	9±2
TN J2009–3040	3.158±0.001	Ly α	5056±1	15.8±1.6	2300±500†	65±7
		C IV λ 1549	6444±1	2.0±2.0	2300±500†	10±1
		He II λ 1640	6815±5	0.65±0.1	1380±500	4±1
		C III] λ 1909	7920±5	3.0±0.4	2900±600†	14±2
MP J2226–7654	0.5500±0.0002	[O II] λ 3727	5776±1	2.8±0.3	400±180	25±3
		CaII K	6098±1	–2.3±0.3	1200±300	–12±2
		CaII H	6161±1	–2.0±0.3	1000±200	–10±2
		[O III] λ 5007	7680±10	1.2±0.2	900±500	4±1
		[O III] λ 5007	7760±5	0.8±0.2	800±600	8±2
MP J2352–6154	1.573±0.003	C IV λ 1549	3990±1	0.7±0.1	800±260	80±16
		He II λ 1640	4223±1	0.40±0.04	<500	40±7
		C III] λ 1909	4900±1	0.30±0.04	<500	31±5
		[Ne IV] λ 2424	6235±1	0.40±0.05	340±200	30±10
		Mg II λ 2800	7200±4	0.3±0.1	600±400	30±10

† Not considering the broad underlying component.